Nanoscale

Accepted Manuscript

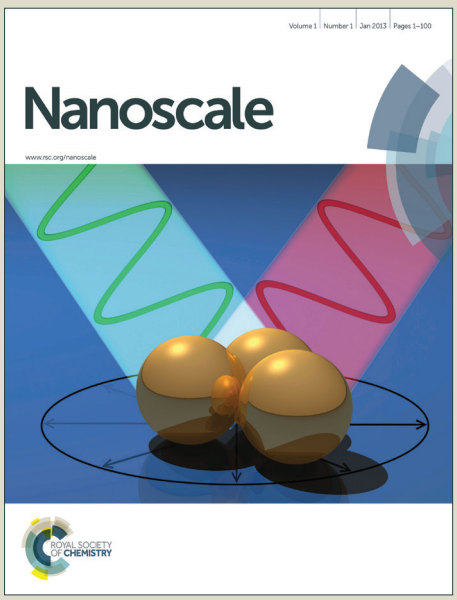

ROYAL SOCIETY OF CHEMISTRY

www.rsc.org/nanoscale

Submitted to Nanoscale, 08/2014

Decoration of Size-Tunable CuO Nanodots on TiO_2 Nanocrystals for Noble Metal-Free Photocatalytic H_2 Production

Geon Dae Moon,[†] Ji Bong Joo,[†] Ilkeun Lee, and Yadong Yin*

Department of Chemistry, University of California, Riverside, CA, 92521, USA

[†]These authors contributed to this work equally.

**Corresponding author. E-mail: yadong.yin@ucr.edu*

Abstract

We report a simple yet effective approach for the decoration of TiO_2 nanocrystal surface with size-tunable CuO nanodots for high-performance noble metal-free photocatalytic H_2 production. Modification with polyacrylic acid enables the surface of TiO_2 nanocrystals to be selectively deposited with $Cu(OH)_2$ nanodots, which can be subsequently converted to CuO through dehydration without changing their morphologies. UV irradiation of the nanocomposite solution in the presence of a hole scavenger produces photogenerated electrons which reduce CuO to metallic Cu nanodots, making them effective co-catalysts in a role similar to Pt for promoting photocatalytic H_2 production. Due to the considerably high work function of Cu, the formation of metal-semiconductor Schottky junction induces efficient charge separation and transfer. As a result, the TiO_2 nanocrystals decorated with an optimal amount of CuO nanodots (1.7 wt%) could reach ~50% of the photocatalytic activity achievable by the Pt-TiO_2 counterparts (1 wt%), clearly demonstrating the great potential of such composite catalysts for efficient noble metal-free photocatalytic H_2 production.

Keywords:

Photocatalyst, TiO_2, CuO, Hydrogen production, Co-catalyst

Introduction

As a green energy carrier, hydrogen generated *via* photocatalytic reaction has attracted much attention due to its high energy capacity, environment friendliness, and sustainability.[1-9] Photocatalytic water splitting is possible only when the conduction band (CB) edge of a semiconductor is more negative than the redox potential of H^+/H_2 (0 V vs. NHE) and the valence band (VB) edge is more positive than the redox potential of O_2/H_2O (1.23 V). In this regard, titanium dioxide (TiO_2, titania) has been recognized as a suitable candidate for photocatalytic water splitting because of its adequate potential window along with its biological and chemical inertness, high oxidizing power, low-cost, and long-term stability against chemical corrosion.[10-13] Nevertheless, hydrogen production efficiency from pure TiO_2 through photocatalytic water splitting reaction has proven to be extremely low owing to the following reasons: 1) high recombination rate of photogenerated electrons and holes, 2) rapid backward reaction of hydrogen and oxygen to form water, and 3) large overpotential for the generation of H_2 on the titania surface.[10, 14] To overcome these shortcomings, several approaches have been explored to enhance the efficiency of charge separation and transport, both conceptually and experimentally, including solid-state *Z*-scheme,[15, 16] *p-n* junction,[17-19] sacrificial reagent,[20] and metal/non-metal co-catalysts.[21-23] Specifically, the deposition of noble or non-noble metal on the surface of TiO_2 has been massively investigated to enhance the efficiency of photocatalytic hydrogen production by inhibiting the recombination between photo-generated electrons and holes.[10] In the presence of noble metals such as Pt, photo-generated electrons can be transferred from the conduction band of TiO_2 to noble metals since the Fermi levels lie below the CB of TiO_2, leading to efficient charge separation by lowering the recombination rate. Accumulation of electrons on the deposited noble metal particles can shift their Fermi level close to the CB of TiO_2, resulting in more negative

energy level than the H_2 evolution potential, which helps water-splitting.[24, 25] According to the Gartnër model,[26] the light-induced charge separation efficiency in metal-semiconductor Schottky junction is related to the space charge layer (depletion layer), which is, in turn, proportional to the work function of metals. Thus, noble metals with high work function are beneficial for higher photocatalytic activity through efficient charge transfer. In this sense, Pt has been widely used, despite the preciousness, as the most efficient co-catalyst for hydrogen evolution when it is deposited in nanoparticle form on TiO_2 surface at an optimal loading (~1 wt%).[27] Due to its rarity, more research has been carried out to replace Pt with low-cost co-catalysts while maintaining comparable enhancement of photocatalytic activity. Cobalt and nickel were found to be effective co-catalysts for hydrogen production, although the photocatalytic activities of the resulting composite catalysts were three times lower than that of Pt-loaded TiO_2.[28, 29] Another inexpensive and active co-catalyst based on copper was also demonstrated to exhibit reasonable photocatalytic activity.[23, 30-37] Different from noble metals, copper nanoparticles loaded on TiO_2 are prone to be easily oxidized under ambient conditions, resulting in the formation of CuO_x-TiO_2, which leads to *p-n* junctions including possibly CuO-TiO_2, Cu_2O-TiO_2, or CuO/Cu_2O-TiO_2 heterostructures.[38] However, often copper oxide or hydroxide nanoparticles on TiO_2 act as a metal co-catalyst rather than *p-n* junction or solid-state *Z*-scheme for hydrogen production under UV irradiation since copper ions can be easily reduced to metallic state due to the electron transfer from the CB of TiO_2.[23, 33]

In this study, we report a new and effective approach to decorate size-controllable CuO nanodots on the surface of TiO_2 nanocrystals by selective precipitation of $Cu(OH)_2$ nanodots onto polyacrylic acid (PAA) modified TiO_2 surface, followed by dehydration to transform $Cu(OH)_2$ into CuO nanoparticles. Unlike conventional impregnation methods which usually end up with

mixtures of several Cu species with uncontrollable size distributions, we have been able to precisely control the size of CuO nanodots from < 1 nm up to 5 nm. Upon UV excitation, the CuO nanodots are further reduced into Cu due to photogenerated electron transfer from the CB of TiO_2 to CuO, leading to the formation of semiconductor-metal Schottky junctions. Our studies on the size-dependent charge equilibration between TiO_2 and metal co-catalyst under UV irradiation has revealed the photocatalytic activity of semiconductor-metal nanocomposites as the smaller size of metal nanoparticles induces the greater shift in the Fermi level to more negative potential with higher photocatalytic activity.[25] The CuO-TiO_2 photocatalyst with optimal loading displays near half of the photocatalytic activity of Pt-loaded TiO_2 catalyst for H_2 evolution under UV irradiation, making the system a promising photocatalyst that does not rely on expensive Pt cocatalyst.

Experimental

Decoration of CuO nanodots on TiO_2 nanocrystals. Commercial Degussa TiO_2 powder (P25) was used as the source of TiO_2 nanocrystals. The surface of TiO_2 was modified with poly(acrylic acid) (PAA, Mw = ~1,800, Aldrich). Typically, TiO_2 powder (1.0 g) was dispersed in deionized water (DI water, 150 mL), mixed with PAA (6.0 g), heated at 95 ºC for 24 h, collected by centrifugation, cleaned by water three times, and redispersed in H_2O (200 mL). In a separate solution, copper (II) nitrate trihydrate ($Cu(NO_3)_2 \cdot 3H_2O$, Sigma-Aldrich, 2.0 g) was dissolved in an ammonium hydroxide solution (125 mL, 28% in H_2O) at room temperature and then heated at 60 °C. Upon the appearance of $Cu(OH)_2$ precipitate on the surface, the solution was filtered by a syringe PTFE filter (pore size: 1.0 μm, Whatman), producing a deep blue precursor solution containing copper-ammonia complexes. For the decoration of $Cu(OH)_2$ nanodots on TiO_2 surface, a certain amount of the Cu precursor solution was added into a PAA-modified TiO_2 solution (22.5

mL). In 1 h, $Cu(OH)_2$-decorated TiO_2 particles were collected by centrifugation, cleaned with water and then ethanol, dried in a vacuum desiccator, and then calcined at 200 ºC for 1h to dehydrate $Cu(OH)_2$ into CuO.

Characterization. The morphology of the samples were investigated using a transmission electron microscopy (TEM, Philips Tecnai 12, 200 kV). Powder X-ray Diffraction (XRD) pattern was obtained on a Bruker D8 Advance diffractometer using Cu Kα radiation. UV-vis diffuse reflectance spectra were measured on dry powders using a UV-Vis spectrophotometer (HR2000CG-UV-NIR, Ocean Optics) with $BaSO_4$ as a reflectance reference. The mass loading of CuO deposited on TiO_2 particles was measured by Inductive Coupled Plasma-Atomic Emission Spectroscopy (ICP-AES, PerkinElmer, Optima 2000 DV). X-ray photoelectron spectroscopy (XPS) characterization was performed by using a Kratos AXIS ULTRA^{DLD} XPS system equipped with a Al Kα monochromated X-ray source and a 165-mm electron energy hemispherical analyzer. The binding energy was calibrated for each sample by referencing the C 1s peak to 284.6 eV.

Photocatalytic hydrogen production. Photocatalytic hydrogen production was carried out in a Pyrex glass reactor. Photocatalysts (5 mg) was well dispersed in an aqueous methanol solution (10 vol%, 50 mL). Based on the relationship between the catalyst amount and the average hydrogen production rate (Figure S10), the amount of 5 mg was chosen to ensure that the reaction is not limited by reactant diffusion and the intrinsic activity of the catalysts can be measured. An Opti-Quip 100 W Hg lamp was used as a light source for UV-vis irradiation. The amount of hydrogen produced was determined by gas chromatography (HP 5890, equipped with a Molecular sieve 5A, Restel, packed column) with a thermal conductivity detector.

Results and Discussion

A chemical transformation process was involved in the preparation of CuO-decorated TiO_2 photocatalysts. In the first step, $Cu(OH)_2$ nanodots were selectively deposited to the surface of PAA-modified TiO_2 nanocrystals by taking advantage of the high pH dependence of the solubility of $Cu(OH)_2$.[39, 40] Initial dissolution of $Cu(NO_3)_2$ in ammonia solution produced a deep blue solution of $Cu(NH_3)_6^{2+}$. Heating the system at 60 °C evaporated NH_3 and gradually reduced its concentration as well as the pH of the solution to the critical point that $Cu(OH)_2$ precipitate started to appear. Mixing such a Cu precursor solution with TiO_2 nanocrystals led to further decrease in the pH due to neutralization by the acidic PAA, promoting the conversion from soluble $Cu(NH_3)_6^{2+}$ to less soluble $Cu(OH)_2$ around the TiO_2 nanocrystal surface. The precipitation was completed within a few seconds. As shown in the TEM image in Figure 1A, very small $Cu(OH)_2$ nanodots have been evenly decorated on the surface of TiO_2 nanocrystals without any apparent coalescence. After being annealed at 200 ºC for 1 h, $Cu(OH)_2$ dehydrated and transformed into CuO (bandgap energy ~1.2 eV), accompanied by a color change from blue to brown (inset images). CuO nanodots remained well dispersed on TiO_2 surface without showing any significant morphological change (Fig. 1B). In contrast, if no TiO_2 nanoparticles were present, bundled $Cu(OH)_2$ nanobelts were obtained, which then can be transformed to CuO nanobelts after dehydration (Fig. S1). PAA is believed to contribute to the formation of only nanodots on the TiO_2 surface by affecting the nucleation and growth of $Cu(OH)_2$, as supported by the fact that unmodified TiO_2 nanocrystals can only initiate the formation of bundled-CuO nanorods (Fig. S2).

To identify the chemical composition of the samples, XPS analysis was carried out. Figure 1C shows the high-resolution Cu 2p spectra of $Cu(OH)_2$- and CuO-decorated TiO_2 nanocrystals. The measured binding energies of Cu $2p_{3/2}$ and Cu $2p_{1/2}$ correspond to 934.6 and 954.3 eV in the $Cu(OH)_2$-decorated TiO_2 sample, indicating the 2+ oxidation state of Cu, which can be assigned to

$Cu(OH)_2$ in light of the previous references.[41] In addition, two shake-up lines located at 943 and 962 eV further confirm the oxidation state of Cu^{2+}. After dehydration in air at 200 ºC, the binding energies of Cu $2p_{3/2}$ and Cu $2p_{1/2}$ moved to 933.6 and 953.6 eV, confirming the transformation from $Cu(OH)_2$ to CuO as suggested in literature.[41]

Photoexcitation in semiconductor nanoparticles causes charge equilibration when they are in contact with metals or other semiconductors to form metal-Schottky or n-n/*p*-*n* junctions. Such a charge distribution change, especially in metal-semiconductor Schottky junction, has direct influence in regulating the energetics of the composites by shifting the Fermi levels to more negative potentials. One factor that can significantly influence the electronic properties of the nanocomposite is the size of the metal particles. Quantized conductance of metal has been investigated to show the size-dependent electronic band structures.[42] Size-dependent shift in the Fermi level of TiO_2-Au nanocomposite was also found to influence the energetics by enhancing the photogenerated charge separation.[25] The greater change in the Fermi level with smaller Au nanoparticles indicated higher photocatalytic reduction efficiency and photocurrent generation. Thus, size control is of great importance for optimizing the photocatalytic activity in nanocomposite photocatalysts. Figure 2 shows TEM images of CuO-decorated TiO_2 nanocrystals synthesized at different CuO loading amounts. For all samples, small CuO nanodots can be clearly seen uniformly dispersed on the surface of TiO_2 nanocrystals. The CuO-TiO_2 composite with 1.1 wt% CuO contained obviously the smallest nanodots. As the loading amount of CuO increases from 2.3 to 7.0 wt%, the size of deposited CuO nanodots became slightly larger (Fig. 2). CuO nanodots with less than 1.0 wt% loading could not be clearly observed on the TiO_2 surface due to their even smaller sizes (Fig. S3). It is noticeable that the average size of the nanodots increased from <1.0 nm to 3.1 nm with loading weight percent and saturated at 7.0 wt% loading. Further

increased loading (e.g. 14 wt%) of CuO caused self-nucleation and led to the formation of large mesoporous CuO bundles (Fig. S4).

Figure 3 shows the UV-vis diffuse reflectance spectra of the samples loaded with different amounts of CuO (0 to 7.0 wt%). The reflectance in visible range decreased with increasing loading of CuO. However, there was no conspicuous difference in the absorption edge between TiO_2 and CuO-TiO_2 samples, implying that CuO was deposited on the TiO_2 surface rather than incorporated into the TiO_2 lattice.

TiO_2 has been considered as an efficient photocatalyst because the conduction band edge of anatase is more negative than the reduction potential of H^+/H_2. When *n*-type TiO_2 and *p*-type semiconductor CuO are in contact, the interfacial band edges bend to facilitate the transfer of photogenerated electrons. While the photogenerated holes may be consumed by scavenging reagent such as methanol, the electrons in CB of TiO_2 accumulate near the interface with CuO due to more positive potential of CB of CuO. Interestingly, fluorescence quenching in CuO-TiO_2 nanocomposite has been demonstrated to guarantee the transfer of photogenerated electrons from TiO_2 to CuO clusters, which can induce the reduction of Cu^{2+} to Cu^0.[43] Figure 4A shows a schematic flow underlying the mechanism of photocatalytic H_2 generation in CuO-decorated TiO_2 nanocrystals. UV irradiation induced the color change from brown to deep green in 30 min, which corresponded to the Cu^0 state for photocatalytic H_2 production (Cu-TiO_2). Interestingly, the Cu-TiO_2 solution gradually turned yellow by re-oxidation in ambient condition for 6 h, which is different from the initial brown color. To investigate the oxidation states of Cu, we compared the Cu 2p peak in initial CuO-decorated TiO_2 and the re-oxidized sample with XPS (Fig. 4B). The peak located at 933.6 eV split into two different peaks at 933.8 (56.5%) and 932.1 (43.5%) eV, indicating the presence of Cu^{1+}. This observation infers that the initial CuO was reduced to Cu by

the transfer of photogenerated electrons under UV light and re-oxidized to the mixture of CuO and Cu_2O due to the high reactivity of copper nanoparticles towards oxygen.[44] Under continuous UV irradiation, Cu nanoparticles on the surface of TiO_2 remain stable and can work as a metal co-catalyst to facilitate charge separation and transfer of the photogenerated electrons from TiO_2 to Cu, where H^+ is reduced to H_2 molecules.

A Schottky barrier is formed when *n*-type semiconductor is in contact with metal containing high work function, which produces a charge depletion region at the junction by constructing an electric field. In the bulk of a solid (far from a junction), no field exists to ensure charge separation. However, the electric field present at the junction allows for charge separation of photogenerated carriers by the intrinsic absorption of light. By neglecting charge recombination in the charge depletion region, the light-induced charge separation efficiency can be calculated as the electrical current flowing across the interface (I) in the following equation:[26]

$$I = e \cdot I_0 \cdot \frac{1 - e^{-\alpha w}}{1 + \alpha \cdot L_m} \qquad (1)$$

Where e, I_0, α, w, and L_m are the electronic charge, the incident light intensity, the absorption coefficient of the semiconductor, the space charge layer width, and the mean diffusion length of major carriers, respectively. In the TiO_2 photocatalyst with metal co-catalyst, the space charge layer width (w) can be expressed as follows:

$$\mathrm{w} = \left[\frac{2 \cdot \varepsilon \cdot \emptyset_b}{e \cdot N_d}\right]^{\frac{1}{2}} \qquad (2)$$

where ϕ_b and N_d are the barrier height at the junction of metal-semiconductor and the carrier density of semiconductor, respectively. The barrier height at the junction is closely related to the work function of metals:

$$\emptyset_b = \emptyset_m - x \qquad (3)$$

Where ϕ_m and x are the work function of metal and the electronic affinity of semiconductor, respectively. According to the above equations, the work function of metal regulates the barrier height at the junction and, in turn, the width of space charge region, which, finally, dictates the photocurrent passing through the metal-semiconductor Schottky junction. These expressions predict a higher charge separation efficiency for metals characterized with large work function (ϕ_b). Therefore, noble metals with high work function (i.e. Pt) can facilitate electron transfer leading to higher photocatalytic activity. In addition, contrary to the bulk work function of metal, the work function of small metal nanoparticles is size-dependent due to quantum effect.[45] Thus, charge equilibration between metal and semiconductor interface can also be size-dependent due to the change of work function, which influences the energetics of metal-semiconductor nanocomposite. The size-dependent photocatalytic activity has been recognized in previous studies for Au nanoparticles in TiO_2, and led to improved photocatalytic activity for catalysts containing optimally-sized Au nanoparticles.[46, 47]

Photocatalytic hydrogen production activity of CuO-decorated TiO_2 nanocomposite was measured under UV irradiation using methanol (10 vol% in H_2O) as a hole scavenger. When a control sample of pure TiO_2 nanocrystals was used as the catalyst, only negligible H_2 production was detected (Fig. 5). This low photocatalytic activity is ascribed to the rapid recombination between electrons in CB and holes in VB in TiO_2 and the large overpotential for the production of H_2. Figure 5A shows the effect of CuO loading amount on photocatalytic hydrogen production with UV irradiation time. With only a small amount of CuO (0.4wt%), a remarkable improvement in activity could be achieved in comparison to bare TiO_2 nanocrystals. Figure 5B plots the H_2 production rate vs. CuO loading. The optimal loading amount of CuO nanodots was found to be at 1.7wt%, above which the activity decreased. Such a dependence of photocatalytic activity on the

loading amount of co-catalyst has been found to be general, probably due to several combined effects: i) the decrease of active sites on TiO_2 surface, ii) opacity and light scattering of TiO_2 by CuO resulting in a decreased passage of irradiation,[48] and iii) increase of nanodot size leading to deterioration of photocatalytic activity.[49]

Typically, Pt is the most efficient co-catalyst on TiO_2 for photocatalytic hydrogen production in the presence of a hole scavenger. Nevertheless, numerous efforts have been undertaken to replace Pt with other co-catalysts due to its rarity. In this sense, earth-abundant element, such as Ni, Co, and Cu, are appropriate alternatives as long as they show reasonable photocatalytic activity. The inset in Fig. 5B shows a comparative bar graph of hydrogen production rate under UV irradiation between CuO- and Pt-decorated TiO_2 nanocrystals. For Pt-decorated TiO_2 nanocrystals, 1wt% of Pt loading was previously found to be optimal.[22] The highest activity achieved in TiO_2 nanocrystals loaded with optimal amount of CuO (1.7wt%) can reach ~50% of the value of a 1wt% Pt-TiO_2 sample, suggesting the great potential of the CuO-TiO_2 composite photocatalyst in hydrogen production.

Conclusion

In summary, we have developed a novel and robust process to decorate size-tunable CuO nanodots on the surface of TiO_2 nanoparticles for efficient photocatalytic H_2 production. Polymeric ligand PAA functionalized on the surface of TiO_2 nanocrystals facilitated the selective precipitation of $Cu(OH)_2$ nanodots on the TiO_2 surfaces. Subsequent dehydration transformed $Cu(OH)_2$ to CuO nanodots without changing their morphologies. Illumination of the solution of the CuO-TiO2 nanocomposites under UV in the presence of a hole scavenger reduced Cu^{2+} to Cu^0, producing metallic Cu nanoparticles which then serve as co-catalysts to assist TiO_2 nanocrystals in

photocatalytic water splitting. Similar to noble metals, the metallic Cu nanoparticles in contact with TiO_2 formed metal-semiconductor Schottky junctions which can effectively lower the exciton recombination rate. As a result, the TiO_2 photocatalyst with optimal CuO loading can achieve ~50% the photocatalytic activity of the Pt-TiO_2 counterpart (1 wt%) for H_2 generation, making the current system one of the ideal candidates for earth-abundant photocatalysts.

Supporting Information

Supporting information includes the TEM images, XPS, and XRD spectra of the samples used in this study.

Acknowldegements

Financial support for this project was provided by the U.S. Department of Energy (DE-FG02-09ER16096).

References

1. A. Fujishima and K. Honda, *Nature*, 1972, **238**, 37-38.
2. K. Maeda and K. Domen, *J. Phys. Chem. Lett.*, 2010, **1**, 2655-2661.
3. A. J. Bard and M. A. Fox, *Acc. Chem. Res.*, 1995, **28**, 141-145.
4. O. Khaselev and J. A. Turner, *Science*, 1998, **280**, 425-427.
5. H. Tang, C. M. Hessel, J. Wang, N. Yang, R. Yu, H. Zhao and D. Wang, *Chem. Soc. Rev.*, 2014, **43**, 4281-4299.
6. J. Qi, K. Zhao, G. Li, Y. Gao, H. Zhao, R. Yu and Z. Tang, *Nanoscale*, 2014, **6**, 4072-4077.
7. S. Wang, L. Yi, J. E. Halpert, X. Lai, Y. Liu, H. Cao, R. Yu, D. Wang and Y. Li, *Small*, 2012, **8**, 265-271.
8. N. Yang, Y. Liu, H. Wen, Z. Tang, H. Zhao, Y. Li and D. Wang, *ACS Nano*, 2013, **7**, 1504-1512.
9. D. Barreca, G. Carraro, V. Gombac, A. Gasparotto, C. Maccato, P. Fornasiero and E. Tondello, *Adv. Funct. Mater.*, 2011, **21**, 2611-2623.
10. M. Ni, M. K. H. Leung, D. Y. C. Leung and K. Sumathy, *Renew. Sust. Energ. Rev.*, 2007, **11**, 401-425.

11. P. V. Kamat, *J. Phys. Chem. C*, 2007, **111**, 2834-2860.
12. M. Zhou, J. Yu, S. Liu, P. Zhai and B. Huang, *Appl. Catal., B*, 2009, **89**, 160-166.
13. J. Ran, J. Zhang, J. Yu, M. Jaroniec and S. Z. Qiao, *Chem. Soc. Rev.*, 2014.
14. Z. Jin, X. Zhang, Y. Li, S. Li and G. Lu, *Catal. Commun.*, 2007, **8**, 1267-1273.
15. H. Tada, T. Mitsui, T. Kiyonaga, T. Akita and K. Tanaka, *Nat. Mater.*, 2006, **5**, 782-786.
16. H. J. Yun, H. Lee, N. D. Kim, D. M. Lee, S. Yu and J. Yi, *ACS Nano*, 2011, **5**, 4084-4090.
17. T. Sreethawong, Y. Suzuki and S. Yoshikawa, *Int. J. Hydrogen Energy*, 2005, **30**, 1053-1062.
18. H. G. Kim, P. H. Borse, W. Choi and J. S. Lee, *Angew. Chem., Int. Ed.*, 2005, **44**, 4585-4589.
19. M. H. Lee, K. Takei, J. Zhang, R. Kapadia, M. Zheng, Y.-Z. Chen, J. Nah, T. S. Matthews, Y.-L. Chueh, J. W. Ager and A. Javey, *Angew. Chem., Int. Ed.*, 2012, **51**, 10760-10764.
20. B. Zieliñska, E. Borowiak-Palen and R. J. Kalenczuk, *Int. J. Hydrogen Energy*, 2008, **33**, 1797-1802.
21. B. Kraeutler and A. J. Bard, *J. Am. Chem. Soc.*, 1978, **100**, 5985-5992.
22. G. R. Bamwenda, S. Tsubota, T. Nakamura and M. Haruta, *J. Photochem. Photobiol. A* 1995, **89**, 177-189.
23. J. Yu and J. Ran, *Energy Environ. Sci.*, 2011, **4**, 1364-1371.
24. M. Jakob, H. Levanon and P. V. Kamat, *Nano Lett.*, 2003, **3**, 353-358.
25. V. Subramanian, E. E. Wolf and P. V. Kamat, *J. Am. Chem. Soc.*, 2004, **126**, 4943-4950.
26. W. W. Gärtner, *Phys. Rev.*, 1959, **116**, 84-87.
27. G. L. Chiarello, M. H. Aguirre and E. Selli, *J. Catal.*, 2010, **273**, 182-190.
28. V. Artero, M. Chavarot-Kerlidou and M. Fontecave, *Angew. Chem., Int. Ed.*, 2011, **50**, 7238-7266.
29. P. D. Tran, L. Xi, S. K. Batabyal, L. H. Wong, J. Barber and J. S. Chye Loo, *Phys. Chem. Chem. Phys.*, 2012, **14**, 11596-11599.
30. M. I. Litter, *Appl. Catal., B*, 1999, **23**, 89-114.
31. T. Montini, V. Gombac, L. Sordelli, J. J. Delgado, X. Chen, G. Adami and P. Fornasiero, *ChemCatChem*, 2011, **3**, 574-577.
32. W. J. Foo, C. Zhang and G. W. Ho, *Nanoscale*, 2013, **5**, 759-764.
33. K. Lalitha, G. Sadanandam, V. D. Kumari, M. Subrahmanyam, B. Sreedhar and N. Y. Hebalkar, *J. Phys. Chem. C*, 2010, **114**, 22181-22189.
34. D. Praveen Kumar, M. V. Shankar, M. Mamatha Kumari, G. Sadanandam, B. Srinivas and V. Durgakumari, *Chem. Commun.*, 2013, **49**, 9443-9445.
35. S. Xu, A. J. Du, J. Liu, J. Ng and D. D. Sun, *Int. J. Hydrogen Energy*, 2011, **36**, 6560-6568.
36. D. Barreca, G. Carraro, A. Gasparotto, C. Maccato, O. I. Lebedev, A. Parfenova, S. Turner, E. Tondello and G. Van Tendeloo, *Langmuir*, 2011, **27**, 6409-6417.
37. D. Barreca, G. Carraro, E. Comini, A. Gasparotto, C. Maccato, C. Sada, G. Sberveglieri and E. Tondello, *J. Phys. Chem. C*, 2011, **115**, 10510-10517.
38. D. Barreca, G. Carraro, A. Gasparotto, C. Maccato, M. Cruz-Yusta, J. L. Gómez-Camer, J. Morales, C. Sada and L. Sánchez, *ACS Appl. Mater. Interfaces*, 2012, **4**, 3610-3619.
39. I. Ichinose, K. Kurashima and T. Kunitake, *J. Am. Chem. Soc.*, 2004, **126**, 7162-7163.
40. S. Ko, J.-I. Lee, H. S. Yang, S. Park and U. Jeong, *Adv. Mater.*, 2012, **24**, 4451-4456.
41. M. C. Biesinger, L. W. M. Lau, A. R. Gerson and R. S. C. Smart, *Appl. Surf. Sci.*, 2010, **257**, 887-898.
42. J. Li, Y. Yamada, K. Murakoshi and Y. Nakato, *Chem. Commun.*, 2001, **0**, 2170-2171.

43. J. Yu, Y. Hai and M. Jaroniec, *J. Colloid Interface Sci.*, 2011, **357**, 223-228.
44. M. Yin, C.-K. Wu, Y. Lou, C. Burda, J. T. Koberstein, Y. Zhu and S. O'Brien, *J. Am. Chem. Soc.*, 2005, **127**, 9506-9511.
45. D. M. Wood, *Phys. Rev. Lett.*, 1981, **46**, 749-749.
46. M. Haruta, *Catal. Today*, 1997, **36**, 153-166.
47. G. R. Bamwenda, S. Tsubota, T. Kobayashi and M. Haruta, *J. Photochem. Photobiol. A* 1994, **77**, 59-67.
48. J. Yu, X. Zhao and Q. Zhao, *Thin Solid Films*, 2000, **379**, 7-14.
49. W. Ho, J. C. Yu, J. Lin, J. Yu and P. Li, *Langmuir*, 2004, **20**, 5865-5869.

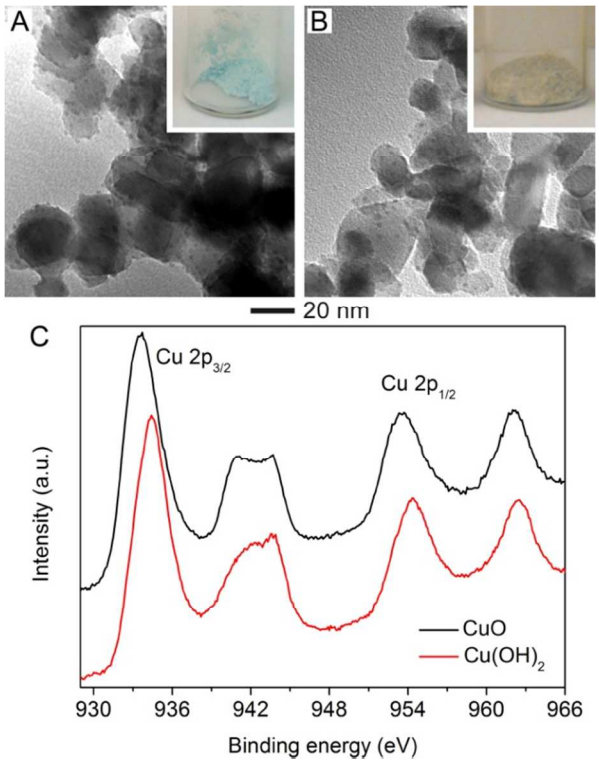

Figure 1. (A, B) TEM images TiO_2 nanocrystals decorated with $Cu(OH)_2$ (A) and CuO (B). The insets are the digital images of corresponding powders. (C) Normalized Cu 2p XPS spectra of $Cu(OH)_2$- and CuO-loaded TiO_2 nanocrystals.

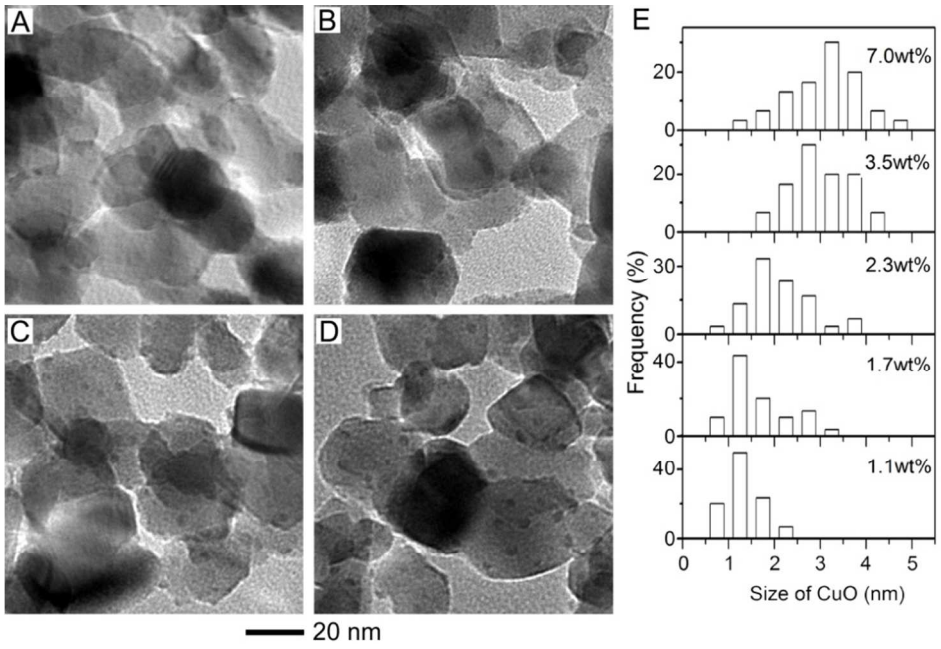

Figure 2. (A-D) TEM images of TiO_2 nanocrystals loaded with different amounts of CuO: (A) 1.1%, (B) 2.3%, (C) 3.5%, and (D) 7%. (E) Size distribution of CuO nanodots on TiO_2 nanocrystals at different loading amounts. About 50 CuO nanodots were surveyed for each sample.

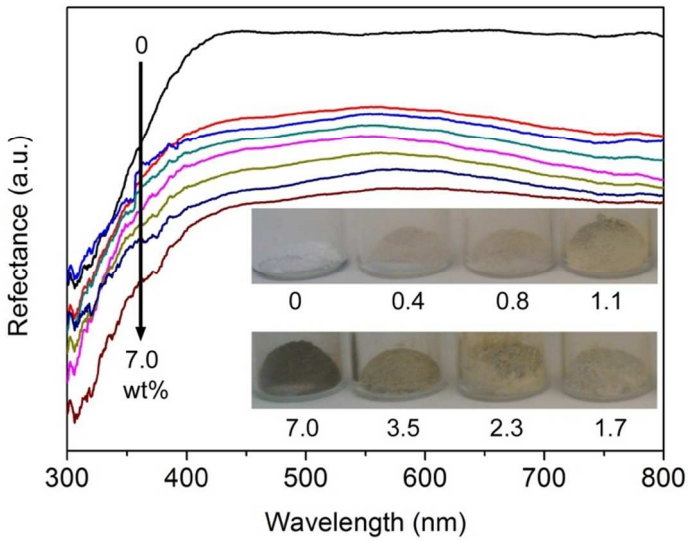

Figure 3. UV-vis diffuse reflectance spectra of CuO-decorated TiO_2 nanocrystals with different loading weight percent from 0 to 7.0%. The insets are corresponding digital images.

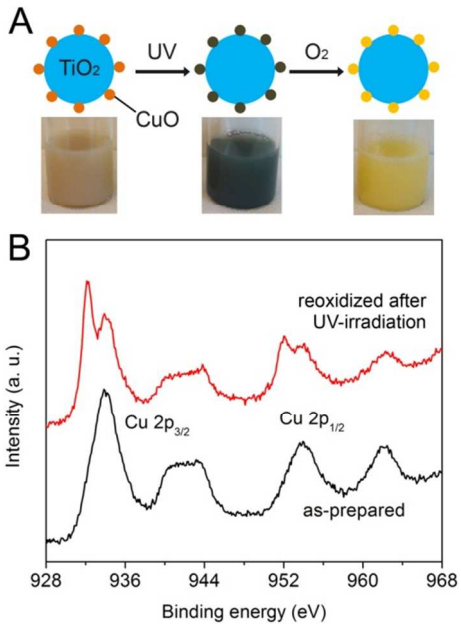

Figure 4. (A) Schematic illustration of photo-reduction of CuO to Cu under UV illumination and then re-oxidation by ambient oxygen. The digital images indicate the corresponding solution color at each state. (B) Normalized Cu 2p XPS spectra of CuO-loaded TiO_2 before and after UV irradiation.

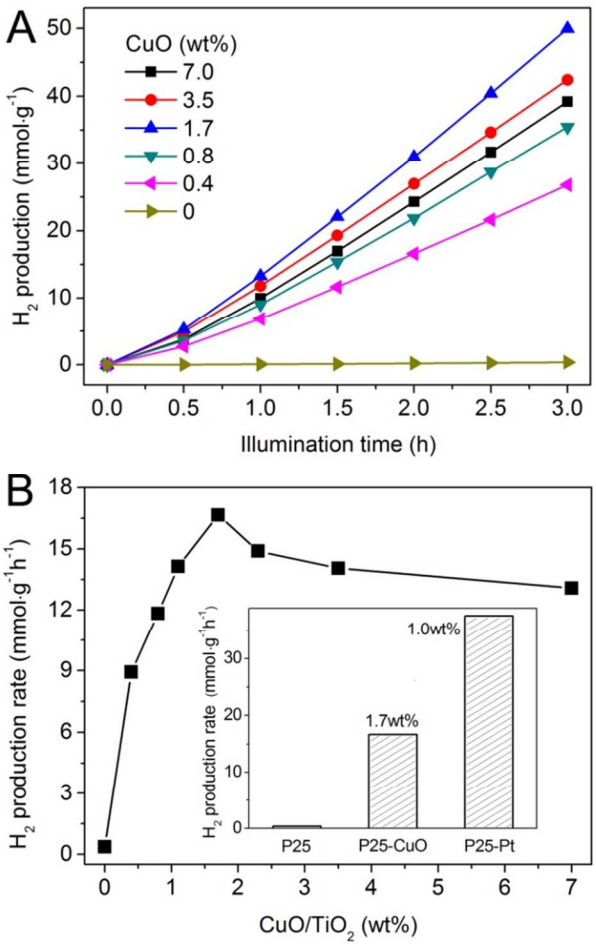

Figure 5. (A) Hydrogen production vs. illumination time in the presence of CuO-decorated TiO_2 catalysts. (B) H_2 production rate vs. loading amount of CuO. The inset in (B) is a bar graph showing the activity of CuO-decorated TiO_2 in comparison to that of Pt-decorated system.

TOC Graphics